Nucleation, Growth, and Overall Transformation Kinetics of Grain Boundary Allotriomorphs of Proeutectoid Alpha in Ti-3.2 At. Pct Co and Ti-6.6 At. Pct Cr Alloys

E. SARATH KUMAR MENON and H. I. AARONSON

The nucleation, growth, and overall transformation kinetics of grain boundary α allotriomorphs were measured in Ti-3.2 at. pct Co and Ti-6.6 at. pct Cr alloys with optical microscopy. Nucleation kinetics were interpreted with classical heterogeneous nucleation theory, using the pillbox model of the critical nucleus. Growth kinetics of allotriomorphs were significantly accelerated by the *rejector* plate mechanism, but much less so than allotriomorphs formed in fcc substitutional matrices at comparable homologous temperatures. Overall transformation kinetics were accounted for with a modified version of Cahn's theory of grain boundary nucleated reactions.

I. INTRODUCTION

GRAIN boundary allotriomorphs are the first morphology to form at most grain boundaries during the proeutectoid α reaction in Ti-X alloys[1] and also in precipitation reactions in many other alloy systems.[2] The suggestion has been made that when allotriomorphs form in substitutional binary alloys, both their nucleation[3] and their growth[4] kinetics will be accelerated less by grain boundary diffusion when the matrix has a bcc structure than when it has an fcc crystal structure. A principal objective of the present investigation was to test experimentally this suggestion, and in the process of doing so, to acquire the first data on both the nucleation and growth kinetics of allotriomorphs which appears to have been reported for any bcc substitutional alloy system.

An additional motivation for the present study was to contribute to understanding why the $\beta \rightarrow \alpha_m$ massive transformation predominates in hypoeutectoid alloys of four Ti-X eutectoid systems[5,6] whereas the proeutectoid α reaction is the only one to occur in such alloys of at least ten other Ti-X eutectoid systems.[1] This was accomplished by comparing the overall kinetics of the two transformation mechanisms in a recently published paper.[7] Since the formation of proeutectoid α allotriomorphs at β grain boundaries precludes the development of the massive transformation in Ti-X alloys (though not during the analogous transformation in β Cu-Zn alloys[8,9]), analysis of the overall transformation kinetics of allotriomorphs alone is sufficient to represent those of the proeutectoid α reaction for the present purpose. Hence, in this paper a modified version[10] of an analysis of grain boundary precipitation due to Cahn[11] is used to combine the data acquired on the nucleation and growth kinetics of α allotriomorphs so as to predict overall transformation kinetics and compare such predictions with experimental measurements.

The Ti-Co and the Ti-Cr alloys used were chosen on the basis of a previous survey,[1] in which their proeutectoid α morphologies were found to be representative of other Ti-X systems and their transformation kinetics were shown to be convenient.

E. SARATH KUMAR MENON, formerly Graduate Student, Department of Metallurgical Engineering and Materials Science, Carnegie Mellon University, Pittsburgh, PA 15213, is Postdoctoral Fellow, Materials Science and Engineering Division, Los Alamos National Laboratory, Los Alamos, NM 87545. H. I. AARONSON is R. F. Mehl Professor, Department of Metallurgical Engineering and Materials Science, Carnegie Mellon University, Pittsburgh, PA 15213.

Manuscript submitted June 10, 1985.

II. EXPERIMENTAL PROCEDURES

The Ti-Co alloy was prepared at the Rockwell International Science Center. A 30 gm alloy button was melted and homogenized at 1273 K in vacuum for 7 days. The composition of the alloy was 3.9 wt pct Co (3.2 at. pct Co) and the total interstitial content was less than 150 ppm. A bar $0.045 \times 0.045 \times 0.225$ m (approximately 2.25 Kg) of the Ti-Cr alloy was obtained from Titanium Metals Corporation of America. This bar was encapsulated in a quartz tube under vacuum (less than 5×10^{-6} torr) and homogenized at 1273 K for 3 days. The homogenized bar was subsequently hot rolled in an inert atmosphere by TIMET to a 0.019 m square bar; this was homogenized at 1273 K for 3 days in vacuum. The composition of the alloy was 7.15 wt pct Cr (6.62 at. pct Cr) and less than 0.039 wt pct Fe. The alloy also contained 340 ppm of O_2 and 30 ppm of N_2. Individual specimens, $0.01 \times 0.01 \times 0.008$ m, were cut from the homogenized alloys for heat treatment. These specimens were wrapped in tantalum foil and encapsulated in Vycor tubes under a vacuum of less than 5×10^{-6} torr after repeated evacuation and flushing with purified helium. Specimens were solution annealed at 1273 K in the β region for 20 minutes. This time was chosen so that the β grain boundaries became perpendicular to the broad faces of the specimens. The solution treated specimens were isothermally reacted in deoxidized, stirred lead baths maintained at the required temperature within ± 1 °C and subsequently quenched in iced water.

The procedure used to measure nucleation kinetics of grain boundary allotriomorphs was recently described in detail.[12] The Schwartz-Saltykov analysis[13,14] is used to convert the number and size distribution of precipitates on the plane of polish to the actual size distribution and the number of allotriomorphs per unit area of grain boundary. From this analysis, the total number of spherical particles of different diameters per unit volume, N_v, in a specimen is related to the number of particles observed in a random two-dimensional section through the relationship:

$$N_v = \frac{1}{\Delta} \sum_{i=1}^{k} \alpha_i n_i \qquad [1]$$

where Δ, the size interval, is given by:

$$\Delta = \frac{\text{largest apparent diameter}}{\text{total number of size groups, } k} \qquad [2]$$

α_i are the coefficients listed in Reference 14 and n_i is the number of particles in each size group.

DeHoff[15] has shown that the Schwartz-Saltykov analysis may be readily extended to particles whose shape can be approximated by ellipsoids of revolution. The resulting equation is identical to Eq. [1], except for a constant shape factor, $k(q)$, which is multiplied by Δ, and whose value depends upon the axial ratio (major axis/minor axis) of the particle, q. In the present situation, experiments showed that the grain boundary allotriomorphs could be satisfactorily approximated as oblate ellipsoids of revolution with an axial ratio of approximately 0.4 and the corresponding shape factor of 0.83.

Figure 1(a) shows the typical appearance of α allotriomorphs formed at β grain boundaries. Measurements were made on microstructures of this type. Figure 1(b) illustrates the situation after extensive sideplate formation has taken place. No measurements were made on microstructures in which sufficient sideplate formation had occurred to alter diffusion fields associated with the allotriomorphs. The grain boundary area per unit volume of specimen, s_v, was obtained from the relation [16]:

$$s_v = \frac{S}{V} = 2\frac{N}{L} \qquad [3]$$

where S is the grain boundary area, V is the volume, and N is the total number of intercepts made by a random test line of total length L with the grain boundaries in the polished section. The number of precipitates per unit area of the grain boundary, N_a, is then obtained from Eqs. [1] and [3] as:

$$N_a = \frac{N_v}{s_v} \qquad [4]$$

The technique used to evaluate the parabolic rate constants for the thickening, α, and the lengthening, β, of grain boundary allotriomorphs has been described by Bradley *et al.*[17] When the matrix grain boundaries are perpendicular to the plane of polish, the length of the longest and the thickness of the thickest allotriomorph represent the true dimensions of allotriomorphs in the size class nucleated first and then sectioned in the plane of the major axis. The relationships between the half-thickness, $S/2$, and the half-length, $L/2$, of the allotriomorphs and the growth time are:

$$\frac{S}{2} = \alpha t^{1/2} \qquad [5]$$

$$\frac{L}{2} = \beta t^{1/2} \qquad [6]$$

III. RESULTS

A. *Nucleation Kinetics*

The allotriomorph density per unit area, N_a, is plotted as a function of isothermal reaction time at the temperatures studied in the Ti-Co (Figure 2(a)) and the Ti-Cr (Figure 2(b)) alloys. Temperature ranges of only 20° and 25 K, respectively, were accessible in these two alloys; similarly narrow temperature regions could be utilized in the previous studies of ferrite allotriomorph nucleation kinetics at austenite grain boundaries in Fe-C alloys.[12,18] The rapid variation of nucleation kinetics with temperature is responsible for increasing the nucleation kinetics from too slow to too rapid to be measured accurately over such small temperature ranges.

As can be seen from the curves in Figure 2, N_a initially increases with time. It then passes through a maximum, probably due to a combination of "hard impingement" among adjacent allotriomorphs, grain growth in the α aggregates thus formed, and the difficulty of revealing impingement boundaries. N_a *vs* time plots for ferrite allotriomorphs also exhibited similar behavior.[12] Because of the rapid transformation kinetics as well as the (inevitable) scatter in the experimental data, discrete intervals of reaction

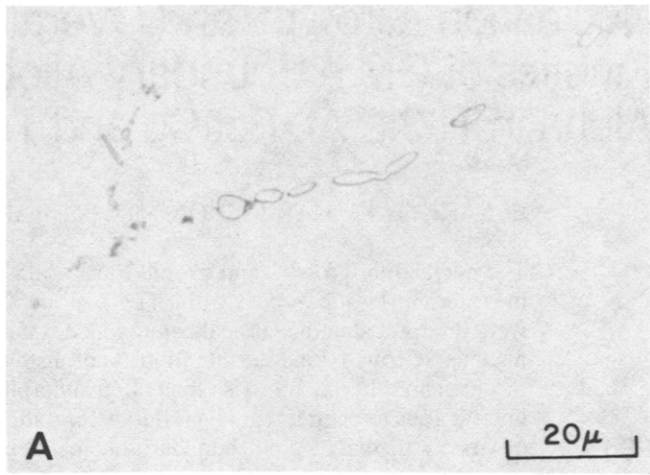

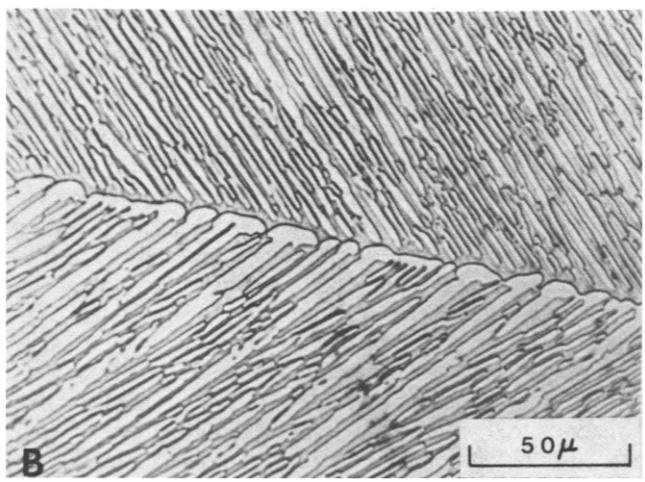

Fig. 1—(*a*) Ti-6.62 at. pct Cr, β solution treated and isothermally reacted at 1008 K for 15 min. (*b*) Ti-3.2 at. pct Co, β solution treated and isothermally reacted at 1033 K for 5 min. These optical micrographs illustrate the typical appearance of grain boundary allotriomorphs observed in this study.

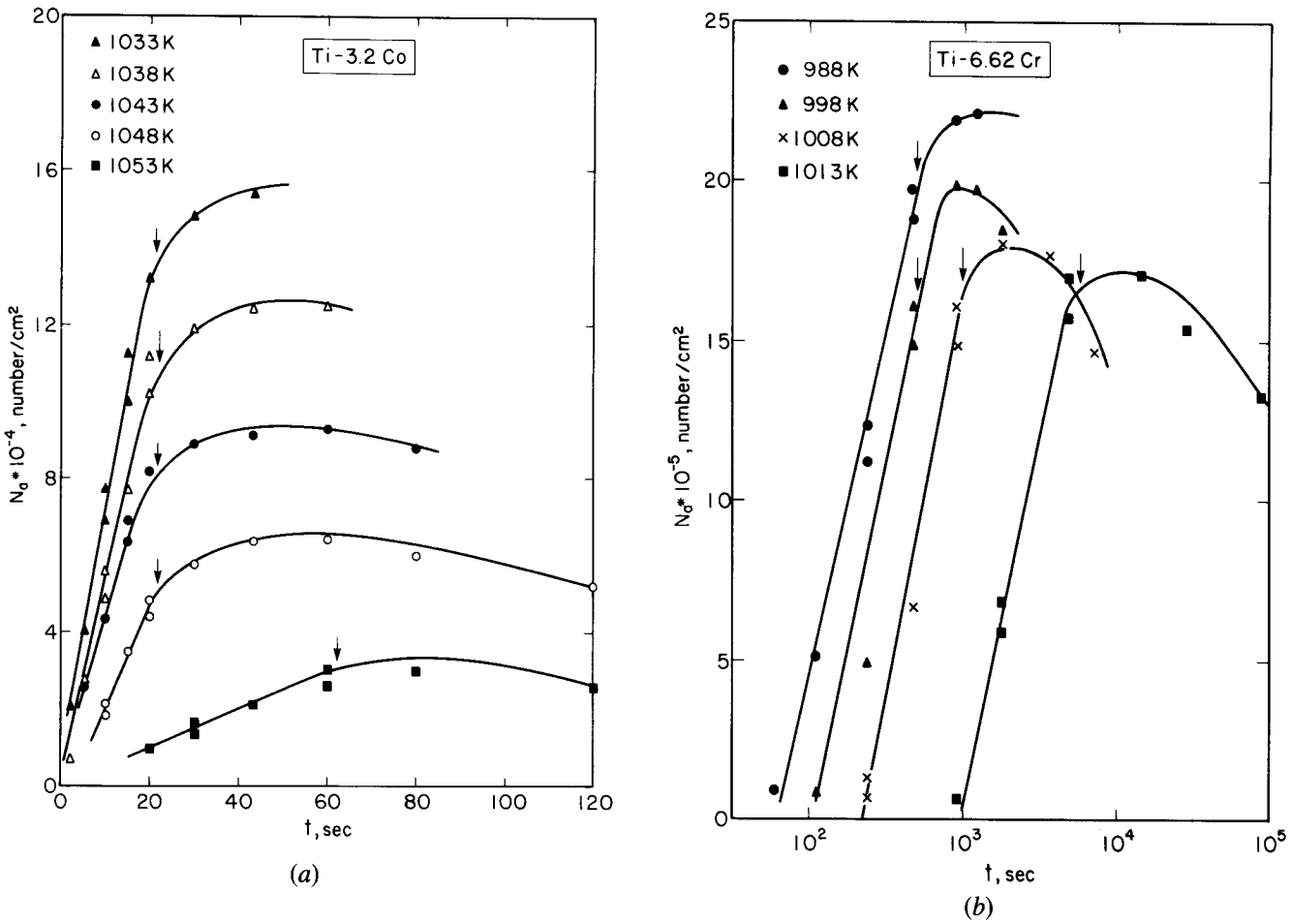

Fig. 2—Plots of N_a, the number of grain boundary allotriomorphs per unit area *vs* reaction time, t, at various temperatures for (*a*) Ti-3.2 at. pct Co and (*b*) Ti-6.6 at. pct Cr. Note that due to the long reaction times involved in the Ti-Cr alloy, a logarithmic scale is used on the time axis. Data points to the left of the arrows were used to evaluate the steady state nucleation rate.

time within which the nucleation rate—given by the slope of these plots—was time-dependent during the early stages of reaction were not observed. Instead, steady state nucleation is seen to have been obtained almost immediately. The steady state nucleation rate J_s^*, was evaluated from the linear least squares slope of the initial portion of these curves. The values thus obtained are summarized in Table I.

B. *Growth Kinetics*

The logarithms of the half-length of the longest and of the half-thickness of the widest grain boundary allotriomorphs are plotted against the logarithm of the isothermal reaction time in Figure 3. The slopes of these plots were calculated by least square analysis. As shown in Figure 4, parabolic growth laws are closely obeyed by the grain boundary allotriomorphs. The parabolic rate constants for lengthening, β, and thickening, α, were evaluated as the slope of the straight lines obtained by least square fitting the half-length and the half-thickness *vs* square root of time data (Figure 5). The parabolic rate constants so evaluated are plotted as a function of reaction temperature in Figure 6 and listed in Table II. The aspect ratio of the grain boundary allotriomorphs, taken as α/β, is seen from Figure 7 to be approximately 0.4 and independent of reaction time and temperature.

Table I. Nucleation Rate Data for α Allotriomorphs

Ti-3.3 At. Pct Co		Ti-6.6 At. Pct Cr	
T (K)	J_s^* (no./cm² sec)	T (K)	J_s^* (no./cm² sec)
1053	470	1013	710
1048	2165	1008	2395
1043	4370	998	4465
1038	5380	988	4775
1033	6920		
β transus: Calculated: 1061.4 K Experimental: 1066 ± 2 K		β transus: Calculated: 1023.5 K Experimental: 1028 ± 2 K	

C. *Overall Transformation Kinetics*

Point counting[19] was used to evaluate the fraction of β matrix transformed to α allotriomorphs as a function of reaction time at each temperature studied in both alloys (Figures 8(a) and (b)). From these plots, TTT curves for the time required to achieve 1 pct transformation to grain boundary allotriomorphs as a function of reaction temperature were constructed (Figures 9(a) and (b)). The dashed curves in these plots were secured using measured nucleation and growth kinetics and Eqs. [31] through [35]. The solid curves were constructed on a primarily theoretical

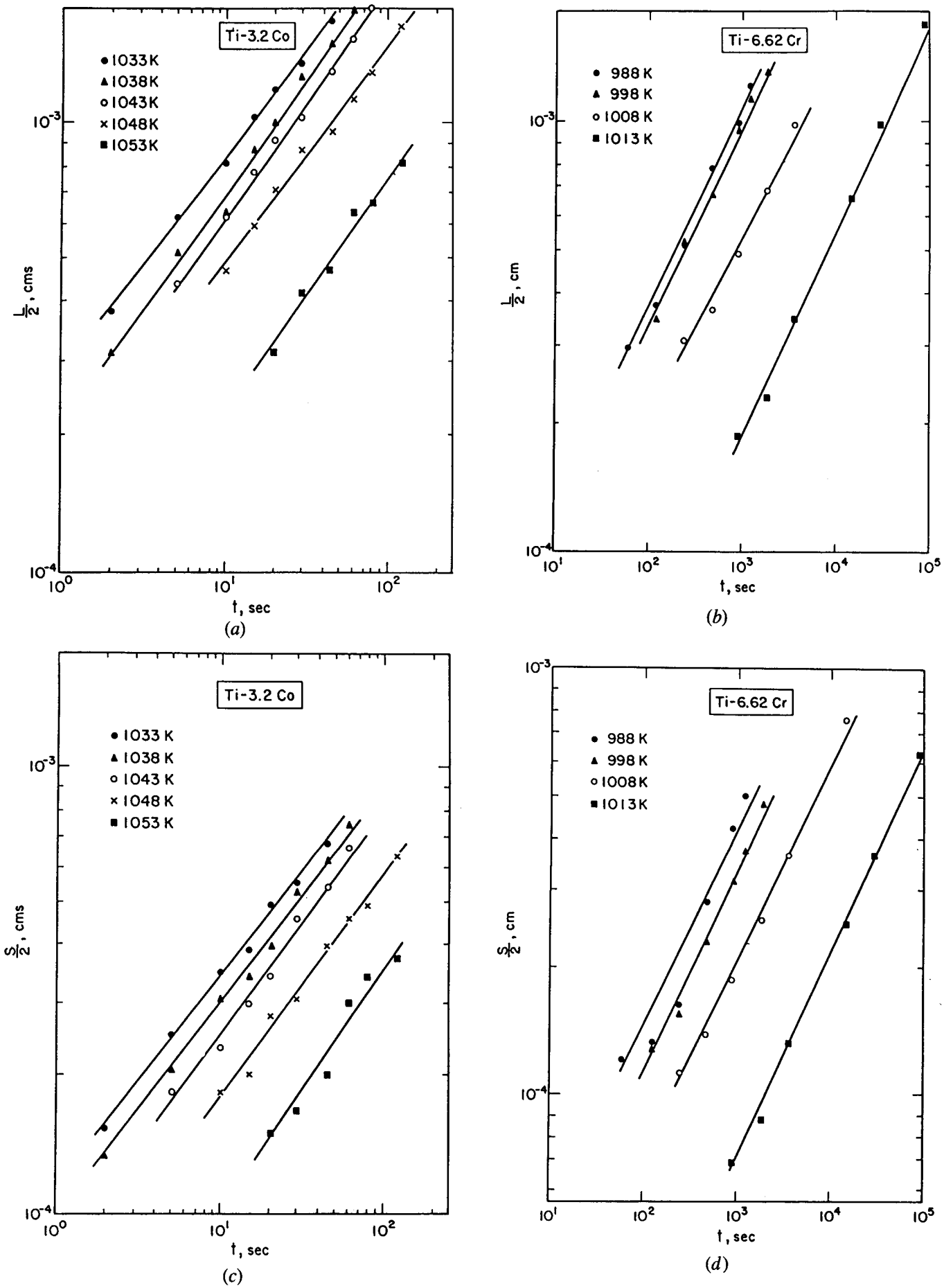

Fig. 3—Log-log plots of half-length, $L/2$, of grain boundary α allotriomorphs *vs* time, t, for (*a*) Ti-3.2 at. pct Co and (*b*) Ti-6.6 at. pct Cr. (*c*) and (*d*) are log-log plots of half-thickness, $S/2$, for the two alloys, respectively.

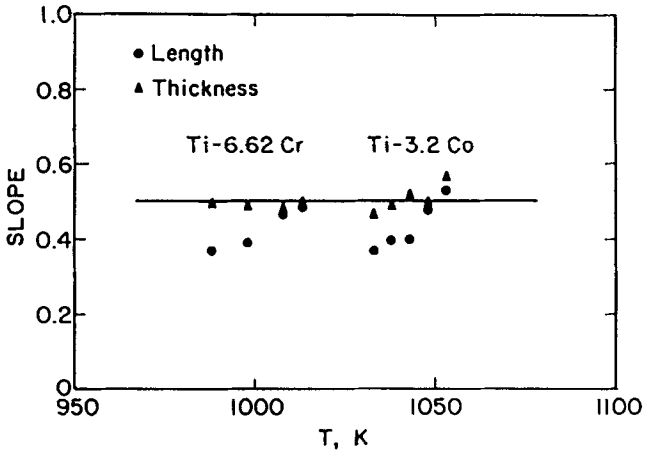

Fig. 4—Plot of the slope of the log-log plots shown in Fig. 3. These are linear least square fitted values.

basis. Equation [15], with experimentally determined parameters, was used to obtain steady state nucleation rates. Equations [28] through [30] were employed to compute the parabolic rate constants for growth, on the assumption that the rejector plate mechanism is not operative (thereby explaining the shift of these curves to longer times relative to the dashed curves). Synthesis of these calculations into $f(t)$ *vs* time curves, and thence into TTT-curves, was again accomplished by means of Eqs. [31] through [35].

IV. DISCUSSION

A. *Analysis of Nucleation Rate Data*

According to classical nucleation theory, the steady state nucleation rate, J_s^*, is expressed by:[20]

$$J_s^* = ZN\beta^* \exp\left(-\frac{\Delta G^*}{kT}\right) \quad [7]$$

where Z is the Zeldovich nonequilibrium factor, β^* is the frequency factor, N is the density of viable atomic nucleation sites, ΔG^* is the free energy of activation for the formation of the critical nucleus, T is the absolute temperature, and k is Boltzmann's constant. Evaluation of Z, β^*, and especially ΔG^* requires that a specific shape be adopted for the critical nucleus. When the crystal structures of the matrix and the precipitate are different, rigorous derivation of the critical nucleus shape for nucleation at grain boundaries—for that matter, even for homogeneous nucleation—has yet to be accomplished.[21] The pillbox morphology, with a broad face co-planar with the grain boundary,[22] which has previously been usefully employed for the proeutectoid ferrite reaction in Fe-C[18] and in Fe-C-X[23] alloys as well as for the massive transformation in Ti-X alloys,[24,25] was therefore adopted. While hardly rigorous, this model, based upon low energy broad faces of the pillbox and a very low energy rim, is demonstrably far superior to the usual double spherical cap and the standard variants thereof.[18,25] This model clearly emphasizes the central role which low energy interfaces play in the formation of critical nuclei which can develop at detectable rates.

Figure 10 illustrates a cross section through the pillbox model; $\gamma^e_{\alpha\beta}$, $\gamma^c_{\alpha\beta}$, and $\gamma^{cb}_{\alpha\beta}$ are the interfacial energies associated with the edge, coherent $\alpha:\beta$ facet within a β grain, and the coherent $\alpha:\beta$ facet at a prior β grain boundary, respectively, and $\gamma_{\beta\beta}$ is the grain boundary energy. Let r and h represent the radius and the height of a cylindrical pillbox-shaped embryo. The free energy change, $\Delta G°$, associated with the formation of the embryo is then:

$$\Delta G° = \pi r^2 h\phi + \pi r^2 \varepsilon + 2\pi r h \gamma^e_{\alpha\beta} \quad [8]$$

with

$$\varepsilon = \gamma^c_{\alpha\beta} + \gamma^{cb}_{\alpha\beta} - \gamma_{\beta\beta} \quad [9]$$

and

$$\phi = \Delta G_v + W \quad [10]$$

where ΔG_v is the volume free energy change accompanying nucleation and W is the strain energy associated with nucleus formation. The critical nucleus shape usually corresponds to the equilibrium shape of the crystal.[20] Assuming with little error[26] that embryos have the same morphology, one may write:

$$\frac{r}{h} = \frac{\gamma^e_{\alpha\beta}}{\varepsilon} \quad [11]$$

Hence ΔG^* may now be derived in the usual manner,[20] together with expressions for r and h applicable to the critical nucleus:[12]

$$\Delta G^* = 4\pi \frac{\gamma^{e^2}_{\alpha\beta}\varepsilon}{\phi^2} \quad [12]$$

$$r^* = -2\frac{\gamma^e_{\alpha\beta}}{\phi} \quad [13]$$

$$h^* = -2\frac{\varepsilon}{\phi} \quad [14]$$

Expressions for Z and β^* are also obtained in a similar fashion;[12] substitution into Eq. [7] yields the steady state nucleation rate for the pillbox model:[12]

Table II. Experimental Parabolic Rate Constants for Growth of α Allotriomorphs

Ti-3.2 At. Pct Co			Ti-6.6 At. Pct Cr		
T (K)	$\alpha \times 10^6$ (m/$\sqrt{\text{sec}}$)	$\beta \times 10^5$ (m/$\sqrt{\text{sec}}$)	T (K)	$\alpha \times 10^6$ (m/$\sqrt{\text{sec}}$)	$\beta \times 10^6$ (m/$\sqrt{\text{sec}}$)
1033	0.982	0.238	988	0.144	0.333
1038	0.935	0.218	998	0.110	0.300
1043	0.850	0.197	1008	0.062	0.167
1048	0.571	0.144	1013	0.021	0.057
1053	0.385	0.077			

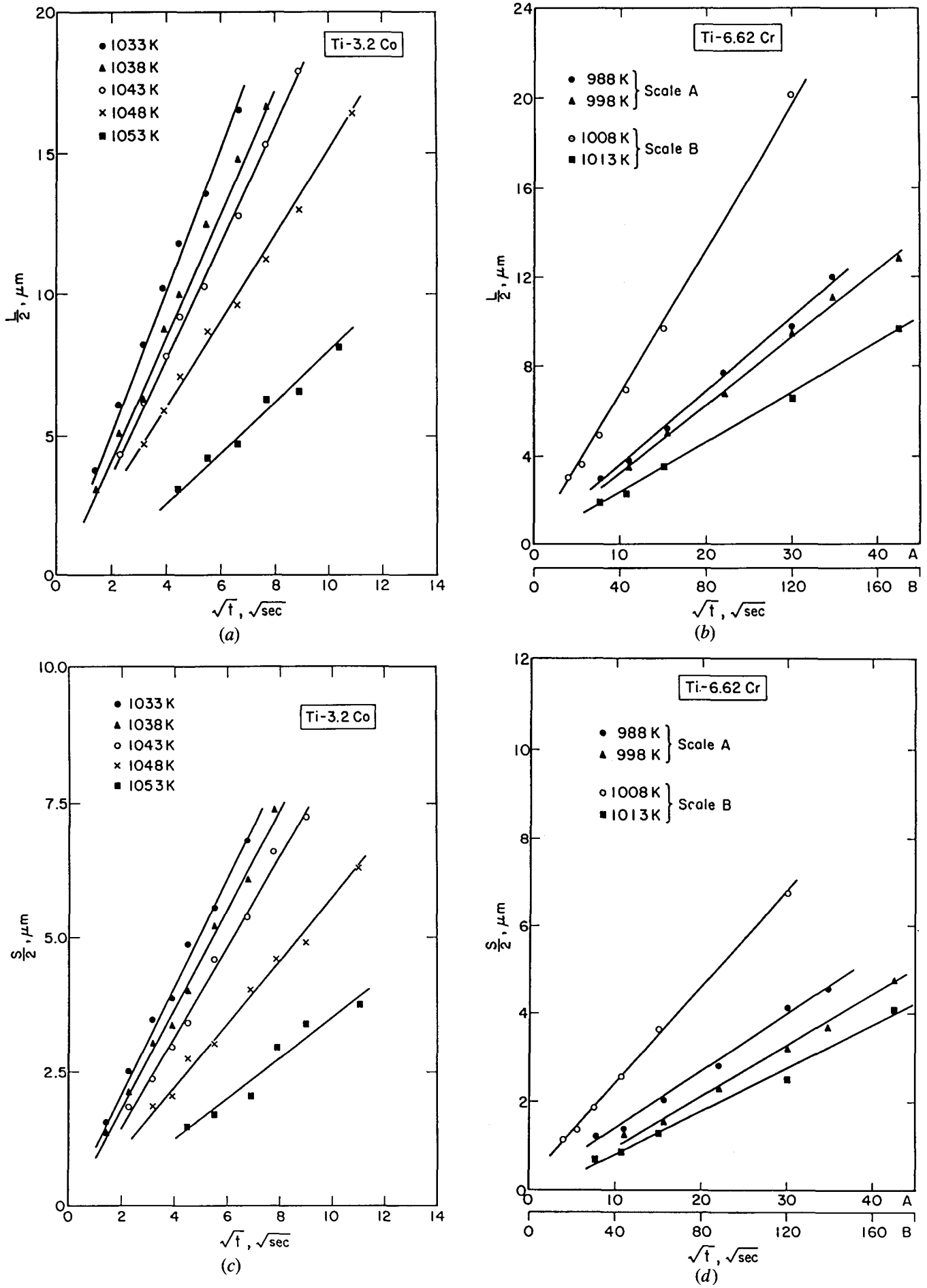

Fig. 5—Plots of half-length, $L/2$, of grain boundary allotriomorphs *vs* $t^{1/2}$, for (*a*) Ti-3.2 at. pct Co and (*b*) Ti-6.6 at. pct Cr. (*c*) and (*d*) are plots of half-thickness, $S/2$, *vs* $t^{1/2}$, for the two alloys, respectively.

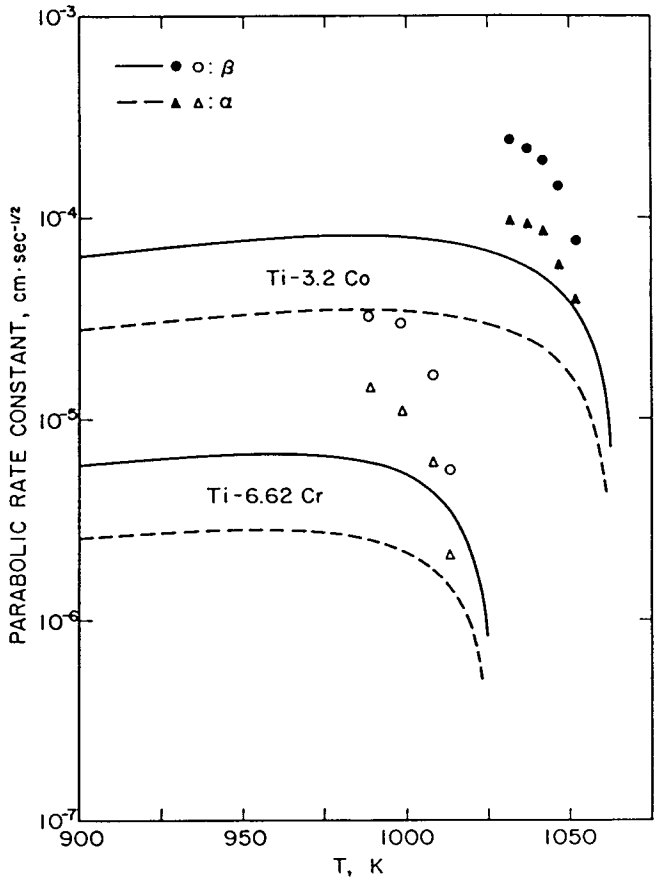

Fig. 6—Parabolic rate constants for lengthening, β, shown by circles and for thickening, α, shown by triangles as a function of isothermal reaction temperature, T, for Ti-3.2 at. pct Co (filled symbols) and for Ti-6.6 at. pct Cr (open symbols). The lines (continuous for β and dashed for α) were calculated from Eqs. [28] through [30].

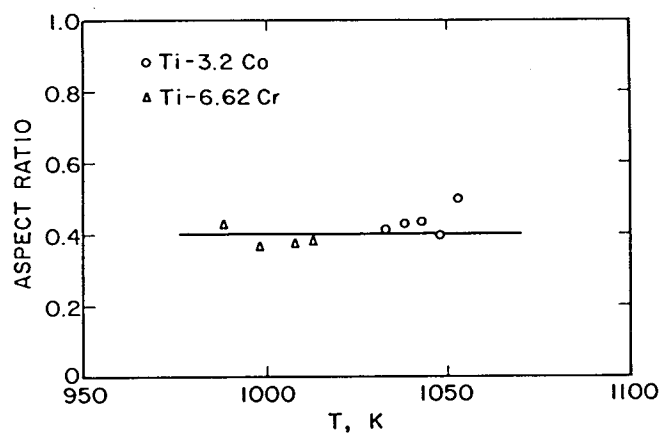

Fig. 7—Plot of the aspect ratio of the grain boundary α allotriomorphs, taken as α/β, as a function of isothermal reaction temperature, T.

$$J_s^* = \frac{2NDX_\beta v_\alpha \sqrt{\varepsilon}}{a_\beta^4 \sqrt{3kT}} \exp\left(-\frac{4\pi\varepsilon\gamma_{\alpha\beta}^{e^2}}{\phi^2 kT}\right) \qquad [15]$$

where D is the diffusivity, X_β is the atom fraction of solute in the β matrix, v_α is the volume per atom of the α phase (17.64×10^{-3} nm^3), and a_β is the lattice parameter of the β phase (0.33132 nm). In the evaluation of ϕ, W is taken

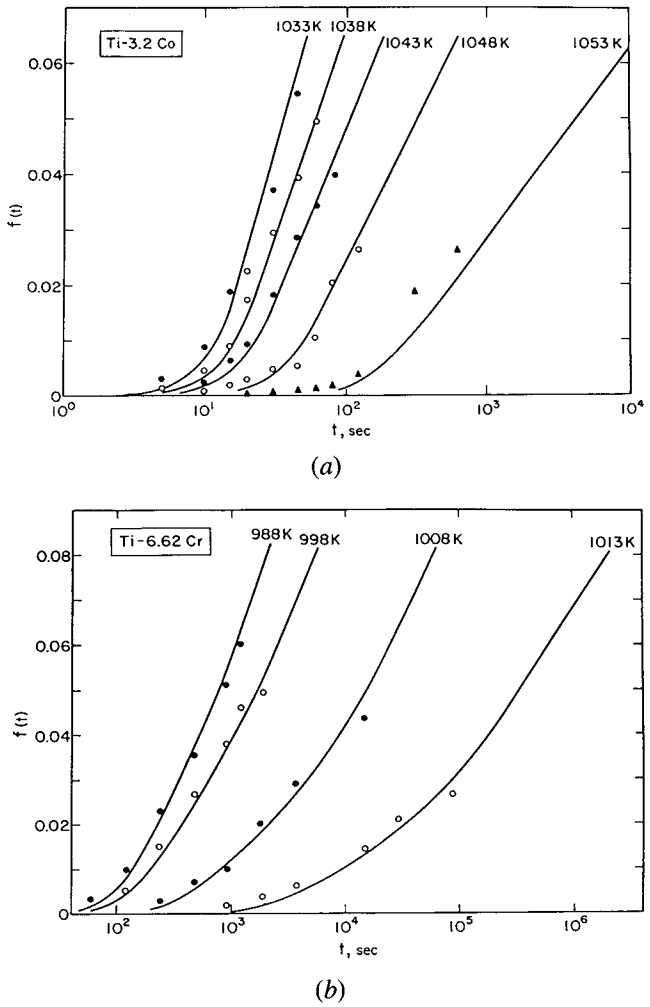

Fig. 8—Plots of fraction, $f(t)$, of the β phase transformed to α allotriomorphs as a function of reaction time, t, at indicated temperatures for (*a*) Ti-3.2 at. pct Co and (*b*) Ti-6.6 at. pct Cr. The lines were calculated from Eqs. [31] through [35].

as negligible, on the ground that it will be largely relaxed into the disordered-type grain boundaries at which nucleation is assumed to occur.[18] Data on the tracer diffusivity of Co^{60} in β-Ti[27] were used, since the error reported in the chemical interdiffusion data of Co in β Ti-Co[28] appears to be very high:

$$D_{Co} = 1.3 \times 10^{-6} \exp\left(\frac{-129300}{RT}\right) \text{m}^2/\text{sec}. \qquad [16]$$

where R is in J/°K · mole. Tracer diffusivities of Cr^{51} in the β phase of Ti-10 wt pct Cr[29] were also employed:

$$D_{Cr} = 2.0 \times 10^{-6} \exp\left(\frac{-168200}{RT}\right) \text{m}^2/\text{sec}. \qquad [17]$$

B. *Calculation of the Volume Free Energy Change Associated with Nucleation*

Analysis of nucleation kinetics requires a precise knowledge of the free energy-composition diagrams for the equilibrium phases. In the case of titanium alloys, experimental thermodynamic data are seldom available. However, recent

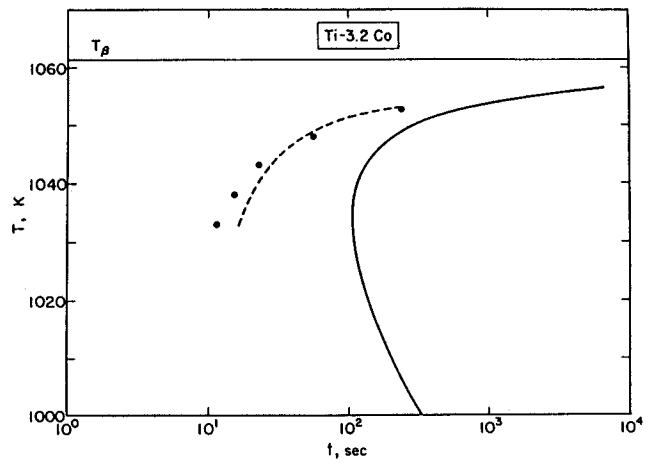

(*a*)

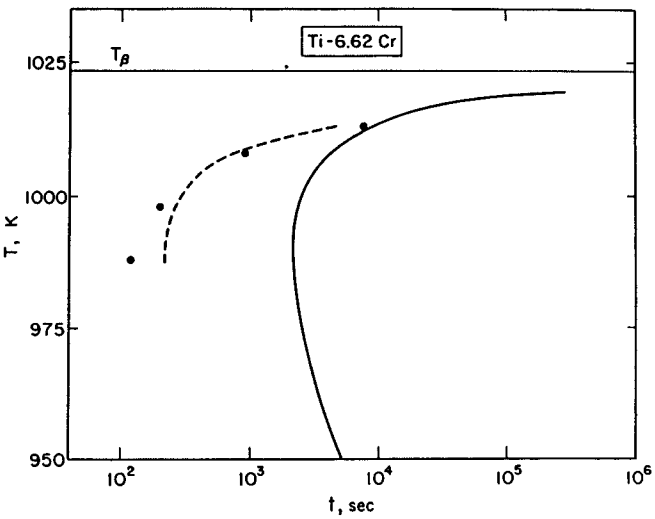

(*b*)

Fig. 9—TTT diagrams for (*a*) Ti-3.2 at. pct Co and (*b*) Ti-6.6 at. pct Cr. T is temperature and t is time. Filled circles represent the time for 1 pct transformation as determined from point counting results. Dashed lines were obtained from Eqs. [31] through [35] using nucleation rates and growth kinetics from Tables I and II, respectively. The continuous lines were obtained from theoretically calculated nucleation rates and growth rates.

developments in phase diagram analysis have made thermodynamic descriptions of a number of binary Ti-X systems available. A summary of the parameters used for the Ti-Cr[30] and the Ti-Co[31] systems is given in Table III.

In order to calculate the driving force associated with critical nucleus formation, the critical nucleus composition was first evaluated by the parallel tangent construction[32,33] which can be expressed as:

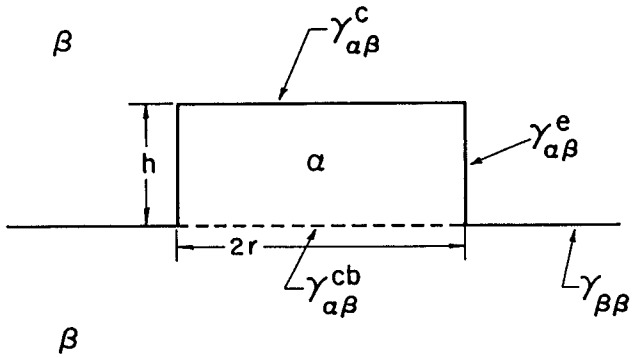

Fig. 10—Schematic diagram illustrating the pillbox-shaped critical nucleus identifying all relevant interfacial energy parameters.

$$\left[\frac{\partial G^\alpha}{\partial X}\right]_{X^*,T} = \left[\frac{\partial G^\alpha}{\partial X}\right]_{X_\beta,T} \qquad [18]$$

For the alloys investigated, whose excess free energies assume the form given in Table III, the critical nucleus composition, X^*, is thus obtained as the solution to the transcendental equation:

$$\begin{aligned} B^\alpha(1-2X^*) + C^\alpha[1-6X^*(1-X^*)] \\ + RT\ln\left[\frac{X^*}{1-X^*}\right] = \Delta G^{\alpha\to\beta}_{\mathrm{Ti}} + \Delta G^{\alpha\to\beta}_j \\ + B^\beta(1-2X_\beta) + C^\beta[1-6X_\beta(1-X_\beta)] \\ + RT\ln\left[\frac{X_\beta}{1-X_\beta}\right] \end{aligned} \qquad [19]$$

In this equation, the subscript j denotes the solute, Co or Cr. The driving force, ΔG_v, associated with nucleation, is then given by:

$$\Delta G_v = G^\alpha|_{X^*} - [(1-X^*)\overline{G}^\beta_{\mathrm{Ti}}|_{X_\beta} + X^*\overline{G}^\beta_j|_{X_\beta}] \qquad [20]$$

where $\overline{G}^\beta_i$ denotes the partial molar free energy of the i^{th} element in the β phase and $G^\alpha|_{X^*}$ is the free energy of the α phase at composition X^*. Noting that the partial molar free energies can be expressed as:

$$\overline{G}^\beta_{\mathrm{Ti}} = G^\beta - X_\beta\left(\frac{\partial G^\beta}{\partial X_\beta}\right) \qquad [21]$$

$$\overline{G}^\beta_j = G^\beta + (1-X_\beta)\left(\frac{\partial G^\beta}{\partial X_\beta}\right) \qquad [22]$$

and using the excess free energy functions given in Table III, ΔG_v is given as:

Table III. Thermodynamic Data for Ti-Co[31] and Ti-Cr[30]

System	B^α	C^α	B^β	C^β
Ti-Co	26000 − 60T	−9000	−9000 − 60T	−9000
Ti-Cr	43403	0	24667 − 6.67T	− 300

$\Delta G^{\alpha\to\beta}_{\mathrm{Ti}} = -4351 + 3.766T$ J/mole
$\Delta G^{\alpha\to\beta}_{\mathrm{Co}} = -6252.5 - 3.766T$ J/mole
$\Delta G^{\alpha\to\beta}_{\mathrm{Cr}} = 8368$ J/mole
$G^{\mathrm{excess}} = X(1-X)[B + C(1-2X)]$
$\Delta G^{\alpha\to\beta}_i$ is the free energy associated with the $\alpha\to\beta$ transformation of element i
B and C are interaction parameters

$$\Delta G_v = (1 - X^*)\Delta G_{Ti}^{\beta\to\alpha} + X^*\Delta G_j^{\beta\to\alpha} + RT\left[(1 - X^*)\ln\left(\frac{1 - X^*}{1 - X_\beta}\right) + X^*\ln\left(\frac{X^*}{X_\beta}\right)\right] + X^*(1 - X^*)[B^\alpha + C^\alpha(1 - 2X^*)] - B^\beta[X_\beta^2(1 - X^*) + X^*(1 - X_\beta)^2] - C^\beta[X_\beta^2(1 - X^*)(3 - 4X_\beta) + X^*(1 - X_\beta)^2(1 - 4X_\beta)] \quad [23]$$

Figure 11 shows ΔG_v for nucleation of α as a function of temperature for the two alloys used in this study.

C. *Calculation of Nucleation Rate as a Function of Temperature*

As noted earlier, the pillbox model of the critical nucleus being employed to analyze the nucleation rate data is unlikely to simulate the critical nuclei actually formed. Further, independently determined values of the energies of the various interphase boundaries taken to form these nuclei are not available. Hence approximations and assumptions must be employed in using this model. Two different methods of doing so are utilized in the present study. The first, due to Enomoto and Aaronson,[34] was evolved from the earlier work of Lange *et al.*[18] The second was developed during the course of the present study in an effort to provide some further improvements. The results of both methods are reported here in order to provide some indication of the magnitude of the uncertainties involved.

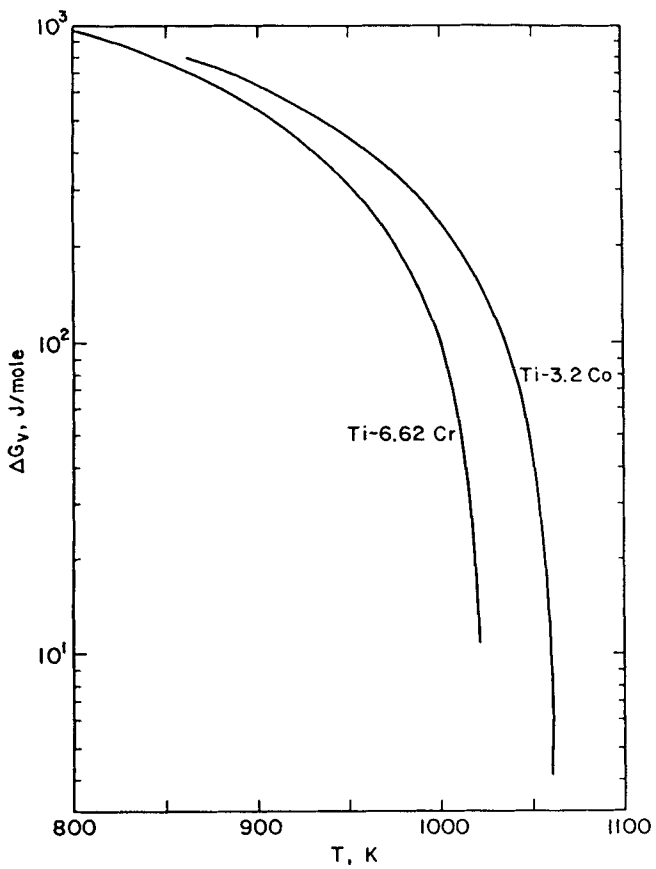

Fig. 11—Thermodynamic driving force for nucleation, ΔG_v, as a function of isothermal reaction temperature, T, calculated according to the parallel tangent construction.

1. *Method 1*

In this method, the height of the pillbox is arbitrarily assigned a value of one unit cell at the lowest temperature used experimentally. From Eq. [14], ε is evaluated at this temperature and then assumed to be the same at all other temperatures. Subsequently, N and $\gamma_{\alpha\beta}^e$ are calculated by the simultaneous solution of Eq. [15] written at two different temperatures, T_1 and T_2. This procedure yields:

$$\gamma_{\alpha\beta}^e = \left\{\ln\left(\frac{D_1 J_2^*\sqrt{T_2}}{D_2 J_1^*\sqrt{T_1}}\right)\right\}^{1/2}\left\{\frac{4\pi\varepsilon}{k}\left(\frac{1}{T_1\phi_1^2} - \frac{1}{T_2\phi_2^2}\right)\right\}^{-1/2} \quad [24]$$

$$N = \left\{\frac{J_1^* a_\beta^4\sqrt{3kT_1}}{2D_1 v_\alpha X_\beta\sqrt{\varepsilon}}\right\}\exp\left(\frac{4\pi\varepsilon\gamma_{\alpha\beta}^{e^2}}{kT_1\phi_1^2}\right) \quad [25]$$

J_s^* can now be evaluated from Eq. [15]. Figure 12 compares the calculated J_s^* *vs* T curves with the experimental data for both alloys. Reasonable agreement is apparent. The ranges of values of $\gamma_{\alpha\beta}^e$ and N obtained from this analysis are shown in Table IV. This table also lists the ε values employed and the spreads of values of h^*, r^*, and $\Delta G^*/kT$, corresponding to the temperature ranges 1000 to 1060 K and 950 to 1020 K for Ti-3.2 at. pct Co and Ti-6.6 at. pct Cr, respectively. The range in values of N was obtained by using the two lowest and the two highest temperatures in Eq. [24]. This method is seen to have yielded at least some values of $\gamma_{\alpha\beta}^e$, N, h^*, r^*, and $\Delta G^*/kT$ that are unacceptably low (Table IV). Hence an alternative method was examined.

2. *Method 2*

The height of the pillbox is now assumed to be independent of temperature. Calculations were performed with $h^* = 1$ and 2 unit cells. The number per unit grain boundary area of viable atomic nucleation sites, N, was varied in the range 10^9 to 10^{20} per m^2. The interfacial energy associated with the edge of the pillbox, $\gamma_{\alpha\beta}^e$, was then calculated from the experimental values of the steady state nucleation rate and the relationship:

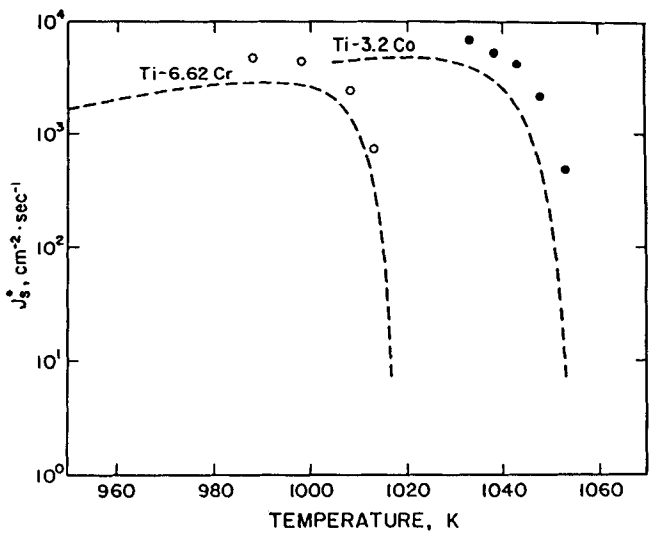

Fig. 12—Steady state nucleation rate, J_s^*, as a function of isothermal reaction temperature. The dashed lines were calculated according to Method 1. ○ and ● represent the experimentally determined nucleation rates for Ti-6.6 at. pct Cr and Ti-3.2 at. pct Co, respectively.

Table IV. Analysis of Nucleation Rates: Method 1

Alloy At. Pct	$\gamma^e_{\alpha\beta}$ (mJ/m^2)	ε (mJ/m^2)	$N \times 10^{-4}$ (No./m^2)	h^* (Unit Cells)	r^* (Unit Cells)	$\frac{\Delta G^*}{kT}$
Ti-3.2 Co	3.5 to 6.0	2.5	0.3 to 0.9	0.4 to 8	1 to 20	0.1 to 10
Ti-6.6 Cr	3.5 to 4.1	3.3	8 to 11	0.4 to 10	0.6 to 13	0.06 to 10

$$\gamma^e_{\alpha\beta} = \left[\ln\left(\frac{2NDX_\beta v_\alpha \sqrt{\varepsilon}}{a_\beta^4 J_s^* \sqrt{3kT}}\right)\right]^{1/2}\left[\frac{4\pi\varepsilon}{\phi^2 kT}\right]^{-1/2} \quad [26]$$

The calculated values of $\gamma^e_{\alpha\beta}$ in the ranges of reaction temperatures employed as a function of h^* and N are listed in Table V. From these results, it is apparent that $\gamma^e_{\alpha\beta}$ is only weakly affected by the choice of N. However, the edge energy appears to be very sensitive to temperature. Hence, unlike previous analyses,[18,12,23,34] where the edge energy was assumed to be independent of temperature, $\gamma^e_{\alpha\beta}$ is taken to vary linearly with temperature; least squares equations fitted to the values obtained from Eq. [26] are included within parentheses in Table V.

The assumption of a linear variation of interfacial energy with temperature can be justified from a thermodynamic point of view. From the Gibbs adsorption Eq. [35]:

$$d\gamma = -S^\gamma dT - \sum_{i=1}^{m} \Gamma_i d\mu_i \quad [27]$$

where S^γ is the excess entropy per unit area of interface, Γ_i is the number of i atoms per unit area, and μ_i is the chemical potential of the i^{th} species. A linear variation of γ with temperature can be expected when solute segregation to the interface is not a marked function of the temperature. The values of $d\gamma/dT$ obtained from this calculation (-0.3 to -0.5 mJ/m^2 · K) are comparable to the experimental values of $d\gamma/dT$ for the average grain boundary energy of the β phase in Ti alloys, *viz.*, -0.10 mJ/m^2 · K for "pure" Ti and -0.65 mJ/m^2 · K in Ti-6Al-4V.[36] Similar linear temperature dependencies have been reported in a variety of metals and alloys.[37]

The J_s^* *vs* T curves calculated on the basis of temperature dependent $\gamma^e_{\alpha\beta}$'s are plotted in Figure 13. Table VI summarizes the ranges of critical nucleus parameters thus secured. All parameters are now seen to have acceptable ranges of values, particularly r^* and $\Delta G^*/kT$.

D. *Analysis of Growth Kinetics*

When volume diffusion controlled, the growth kinetics of grain boundary allotriomorphs are customarily approximated[4,38] as those of oblate ellipsoids of revolution. The solution to this diffusion problem is a specialized form of the one developed by Ham[39] and by Horvay and Cahn.[40] How-

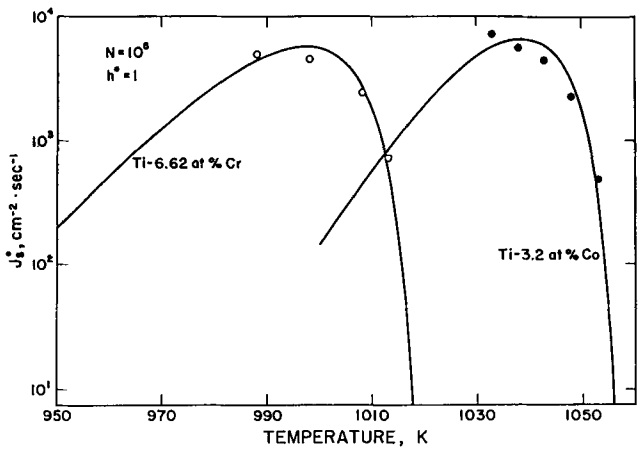

Fig. 13—Steady state nucleation rate, J_s^*, as a function of isothermal reaction temperature. The lines were calculated according to Method 2.

Table V. Calculated Ranges of Edge Energy, $\gamma^e_{\alpha\beta}$, in mJ/m^2

	Ti-3.2 At. Pct Co		Ti-6.6 At. Pct Cr	
N per m^2	$h^* = 1$	$h^* = 2$	$h^* = 1$	$h^* = 2$
10^9	24.6 to 14.8 (529 − 0.49T)	17.6 to 10.6 (381 − 0.35T)	24.0 to 14.0 (419 − 0.40T)	17.3 to 10.1 (303 − 0.29T)
10^{11}	29.0 to 17.0 (645 − 0.60T)	20.7 to 12.2 (462 − 0.43T)	29.7 to 16.8 (535 − 0.51T)	21.2 to 12.0 (383 − 0.37T)
10^{14}	34.6 to 20.0 (788 − 0.73T)	24.6 to 14.2 (562 − 0.52T)	36.9 to 21.1 (657 − 0.63T)	26.3 to 15.1 (469 − 0.45T)
10^{19}	42.3 to 24.0 (982 − 0.91T)	30.0 to 17.0 (698 − 0.65T)	46.1 to 26.1 (836 − 0.80T)	32.8 to 18.5 (595 − 0.57T)

Table VI. Analysis of Nucleation Rates: Method 2

Alloy At. Pct	$\gamma^e_{\alpha\beta}$ (mJ/m^2)	ε (mJ/m^2)	$N \times 10^{-4}$ (No./m^2)	h^* (Unit Cells)	r^* (Unit Cells)	$\frac{\Delta G^*}{kT}$
Ti-3.2 Co	41 to 12	5.4 to 0.3	10^9	1	7 to 94	>12
Ti-6.6 Cr	39 to 11	7.0 to 0.3	10^9	1	6 to 69	> 9

ever, this solution includes an integral which Horvay and Cahn[41] evaluate by means of one series expansion for low aspect ratios and another expansion for aspect ratios near unity. Recently, it was shown that the integral could be evaluated and expressed in terms of the familiar error function.[42] The parabolic rate constants for thickening, α, and for lengthening, β, are written as:[42]

$$\alpha = 2R\sqrt{\Omega D} \quad [28]$$

$$\beta = 2\sqrt{\Omega D} \quad [29]$$

where R is the aspect ratio of the oblate ellipsoid, D is the volume diffusivity, and Ω is a parameter denoting the precipitate:matrix interface and can be obtained by solving the transcendental equation:[42]

$$2e^{\Omega}\Omega^{3/2}\left[\frac{e^{-\Omega}}{\Omega^{1/2}} - \sqrt{\pi}\ \mathrm{erfc}\{\sqrt{\Omega}\}\right] = \frac{X_{\beta}^{\beta\alpha} - X_{\beta}}{X_{\beta}^{\beta\alpha} - X_{\alpha}^{\alpha\beta}} \quad [30]$$

where $X_{\beta}^{\beta\alpha}$ and $X_{\alpha}^{\alpha\beta}$ are the atom fractions of solute in β at the $\beta/(\alpha + \beta)$ phase boundary and in α at the $\alpha/(\beta + \alpha)$ phase boundary at a given temperature and X_{β} is the alloy composition. The phase boundary compositions were obtained by using the data in Table III and by the numerical solution of the simultaneous nonlinear equations expressing the equality of partial molar free energies of the components at various temperatures.

The theoretically calculated and experimentally determined parabolic rate constants for the two alloys used in this study are compared in Figure 6. The experimental parabolic rate constants are seen to lie increasingly above those calculated with decreasing reaction temperature. This result strongly suggests that growth of α allotriomorphs is significantly aided by the "rejector plate" mechanism, the solute-poor precipitate version of the "collector plate" mechanism.[43] According to this mechanism, solute diffuses away from α allotriomorphs along disordered areas of $\alpha:\beta$ boundaries into the adjacent β grain boundary, and then by volume diffusion into the β matrix grains forming this boundary. This deduction is supported by calculating an apparent diffusivity, D_{app}, from Eqs. [28] and [30] through substitution of the experimental parabolic rate constants.[4] Comparison with the independently obtained volume diffusivities (Eqs. [19] and [20]), D_v, in Table VII shows that the ratio D_{app}/D_v increases with decreasing temperature. This is just the behavior previously reported for the growth kinetics of grain boundary θ allotriomorphs in Al-4 wt pct Cu.[4,43]

In order to compare in approximate fashion the effectiveness of interfacial diffusion-aided growth of grain boundary allotriomorphs in the present bcc alloys with that in fcc alloys, the approach of Goldman *et al.*[4] is employed. Using the solidus temperature at the bulk alloy composition as T_m, and the average temperature of the narrow temperature ranges available for growth kinetics measurements as T, Table VII shows that in Ti-6.6 at. pct Cr at $T/T_m = 0.53$, $D_{app}/D_v \approx 32$, and in Ti-3.2 at. pct Co, at $T/T_m = 0.58$, $D_{app}/D_v \approx 15$. Referring to Figure 7 of Goldman *et al.*[4] D_{app}/D_v for Al-4 wt pct Cu (where the matrix is fcc α phase) at $T/T_m = 0.55$ is $\approx$700. Thus the collector/rejector plate mechanism appears to be less effective when the matrix has a bcc structure than when it is fcc at a given homologous temperature, doubtless because D_b/D_v (where D_b is the grain boundary diffusivity) is smaller in bcc metals[44,45] as a consequence of the less dense packing in the bcc lattice.

Analyses have been developed for obtaining grain boundary and interphase boundary diffusivities from growth kinetics when the collector/rejector plate mechanism is the dominant contributor to mass transport.[43,4,46] However, these diffusivities appear in combination with the solute concentration within the interfaces in the analyses. Different estimates of these solute concentrations can lead to drastically different interfacial diffusivities and activation energies for these diffusivities.[43,46,47] Since this problem has yet to be resolved either experimentally or theoretically, calculation of grain boundary and interphase boundary diffusivities attending the growth of α allotriomorphs by the rejector plate mechanism is foregone for the present. The results reported for D_{app}/D_v have accomplished our objective of securing at least an initial comparison of the efficacy of the collector/rejector plate mechanism in a bcc matrix with that in an fcc matrix.

E. *Analysis of f(t) vs t and TTT Diagrams*

Comparison between theory and experiment is made by using the modified version[10] of the analysis of overall transformation kinetics of grain boundary nucleated reactions developed by Cahn.[11] Obara *et al.*[10] calculated the volume fraction, $f(t)$, of the matrix transformed to grain boundary allotriomorphs as a function of reaction time by modeling these precipitates as oblate ellipsoids growing with parabolic kinetics and constant aspect ratio. The resulting equations are:[10]

$$f(t) = 1 - \exp[-b^{-1/2}f(a)] \quad [31]$$

$$a = \sqrt{J_s^*}\,\alpha t \quad [32]$$

$$b = \frac{J_s^* t}{4R^2 S^2} \quad [33]$$

Table VII. Calculated Apparent Diffusivities during Allotriomorph Growth

T (K)	$\frac{D_{app}}{D_v}$*	$\frac{D_{app}}{D_v}$**	T (K)	$\frac{D_{app}}{D_v}$*	$\frac{D_{app}}{D_v}$**
1033	14.8	15.7	988	31.0	36.2
1038	14.6	16.7	998	31.6	26.5
1043	14.8	17.2	1008	14.9	12.7
1048	10.7	10.5	1013	2.5	2.2
1053	4.9	7.6			

*—calculated from lengthening kinetics
**—calculated from thickening kinetics

$$f(a) = a\int_0^1 \left\{1 - \exp\left[-\pi a^2\left(\frac{1}{2}m^4 - m^2 + \frac{1}{2}\right)\right]\right\} dm \quad [34]$$

$$m = \frac{y}{\alpha\sqrt{t}} \quad [35]$$

where y is the perpendicular distance between the grain boundary plane and the plane of polish.

The solid curves in Figures 8(a) and (b) were calculated from Eqs. [31] to [35] and the measured values of J_s^* and α. These curves are seen to provide a good accounting for most of the experimental data points on fraction transformed. Appreciable differences between the calculated curve and experiment occurred only when the Ti-Co alloy was reacted at 1053 K. This is probably due to extensive Widmanstätten precipitation during early stages of the transformation which interfered with the growth of the grain boundary allotriomorphs.

TTT curves for $f(t) = 0.01$ were constructed from the calculated $f(t)$ *vs* t curves and are presented in Figures 9(a) and (b). Reasonable agreement is seen to have been obtained between the experimentally determined data points for $f(t) = 0.01$ and those calculated. However, in both of the alloys, there seems to be a moderate tendency for the calculated curves to lie at longer reaction times than the experimental data at lower reaction temperatures. These discrepancies are the reverse of those found by Obara *et al.*,[10] who ascribed their differences to overlapping of the carbon diffusion fields associated with adjacent ferrite allotriomorphs. Reexamination of Figures 8(a) and (b) at $f(t) \leq 0.01$ indicates an equivalent tendency of the calculated isothermal reaction curves to lie at longer times than the experimental data points, but also suggests that these differences may have arisen from small systematic errors associated with the very low levels of transformation involved.

V. CONCLUSIONS

This study demonstrates that the isothermal transformation kinetics of the proeutectoid α reaction in Ti-X alloys can be adequately described in terms of existing theoretical models. The pillbox-shaped critical nucleus (with an associated edge energy as the unknown parameter), in spite of being a mainly empirical model, can still be used to effect a reasonable evaluation of nucleation kinetics parameters. The observed nucleation kinetics of grain boundary α allotriomorphs can be explained in terms of a temperature-dependent edge energy. The growth kinetics of grain boundary α allotriomorphs are shown to be accelerated by interfacial diffusion *i.e.*, by a *rejector* plate mechanism, though as predicted earlier,[4] not nearly as much as in an fcc matrix at the same homologous temperature. By employing a modified[10] version of an analysis of the overall fraction of the matrix transformed during grain boundary nucleated reactions due to Cahn,[11] the TTT curves for the initiation of the proeutectoid α reaction in Ti-X alloys were calculated from the measured data on allotriomorph nucleation and growth kinetics. These curves compared favorably with those independently determined by point counting.

ACKNOWLEDGMENTS

The authors express their appreciation for the support of the Air Force Office of Scientific Research through Grant #AFOSR-74-2595E.

REFERENCES

1. G. W. Franti, J. C. Williams, and H. I. Aaronson: *Metall. Trans. A*, 1978, vol. 9A, p. 1641.
2. H. I. Aaronson: *The Mechanism of Phase Transformations in Metals*, Institute of Metals, London, 1956, p. 47.
3. G. Vander Velde, J. A. Velasco, K. C. Russell, and H. I. Aaronson: *Metall. Trans. A*, 1976, vol. 7A, p. 1472.
4. J. Goldman, H. I. Aaronson, and H. B. Aaron: *Metall. Trans.*, 1970, vol. 1, p. 1805.
5. M. R. Plichta, J. C. Williams, and H. I. Aaronson: *Metall. Trans. A*, 1977, vol. 8A, p. 1885.
6. W. J. Rensch, R. D. Stauffer, A. E. Backman, and M. R. Plichta: *J. of Met.*, 1983, vol. 35, No. 8, p. 51.
7. E. S. K. Menon and H. I. Aaronson: *Materials Science Forum*, 1985, vol. 3, p. 211.
8. D. Hull and R. D. Garwood: *The Mechanism of Phase Transformations in Metals*, Institute of Metals, London, 1956, p. 219.
9. T. B. Massalski: *Phase Transformations*, H. I. Aaronson, ed., ASM, Metals Park, OH, 1970, p. 433.
10. T. Obara, W. F. Lange, III, H. I. Aaronson, and B. E. Dom: *Proceedings of an International Conference on Solid-Solid Phase Transformations*, H. I. Aaronson, D. E. Laughlin, R. F. Sekerka, and C. M. Wayman, eds., TMS-AIME, Warrendale, PA, 1983, p. 1105.
11. J. W. Cahn: *Acta Metall.*, 1956, vol. 4, p. 449.
12. W. F. Lange, III: Master's Thesis, Michigan Technological University, Houghton, MI, 1977.
13. S. A. Saltykov: *Stereometric Metallography*, 2nd ed. (in Russian), Metallurgizdat, Moscow, 1958.
14. R. T. DeHoff and F. N. Rhines: *Quantitative Microscopy*, McGraw-Hill, New York, NY, 1968, p. 162.
15. R. T. DeHoff: *TMS-AIME*, 1962, vol. 224, p. 474.
16. C. S. Smith and L. Guttman: *TMS-AIME*, 1953, vol. 197, p. 81.
17. J. R. Bradley, J. M. Rigsbee, and H. I. Aaronson: *Metall. Trans. A*, 1977, vol. 8A, p. 323.
18. W. F. Lange, III: Ph.D. Dissertation, Michigan Technological University, Houghton, MI, 1979.
19. J. E. Hilliard and J. W. Cahn: *TMS-AIME*, 1961, vol. 221, p. 344.
20. H. I. Aaronson and J. K. Lee: *Lectures in the Theory of Phase Transformations*, H. I. Aaronson, ed., TMS-AIME, New York, NY, 1975, p. 83.
21. H. I. Aaronson and K. C. Russell: *Proceedings of an International Conference on Solid-Solid Phase Transformations*, H. I. Aaronson, D. E. Laughlin, R. F. Sekerka, and C. M. Wayman, eds., TMS-AIME, Warrendale, PA, 1983, p. 371.
22. W. T. Reynolds, Jr., M. Enomoto, and H. I. Aaronson: *Proceedings of an International Conference on Phase Transformations in Ferrous Alloys*, A. R. Marder and J. I. Goldstein, eds., TMS-AIME, New York, NY, 1984, p. 155.
23. M. Enomoto: Ph.D. Dissertation, Carnegie Mellon University, Pittsburgh, PA, 1982.
24. M. R. Plichta, W. A. T. Clark, and H. I. Aaronson: *Metall. Trans. A*, 1984, vol. 15A, p. 427.
25. M. R. Plichta, J. H. Perepezko, H. I. Aaronson, and W. F. Lange, III: *Acta Metall.*, 1980, vol. 28, p. 1031.
26. W. C. Johnson, C. L. White, P. E. Marth, P. K. Ruf, S. M. Tuominen, K. D. Wade, K. C. Russell, and H. I. Aaronson: *Metall. Trans. A*, 1975, vol. 6A, p. 911.
27. J. Askill and G. B. Gibbs: *Phys. Stat. Sol. (a)*, 1965, vol. 11, p. 557.
28. P. J. M. van der Straten, G. f. Bastin, F. J. J. van Loo, and G. D. Reick: *Zeit. Metallkde.*, 1976, vol. 67, p. 152.
29. A. J. Mortlock and D. H. Tomlin: *Phil. Mag.*, 1959, vol. 4, p. 628.
30. J. L. Murray: *Bull. of Alloy Phase Dia.*, 1981, vol. 2, p. 174.
31. J. L. Murray: *Bull. of Alloy Phase Dia.*, 1982, vol. 3, p. 74.
32. M. Hillert: *Acta Metall.*, 1953, vol. 1, p. 764.
33. M. Hillert: *Jernkont. Ann.*, 1957, vol. 141, p. 757.
34. M. Enomoto and H. I. Aaronson: *Metall. Trans. A*, 1986, vol. 17A, p. 1385.

35. C. H. P. Lupis: *Chemical Thermodynamics of Materials*, Elsevier Science Publishing Co., New York, NY, 1983, p. 360.
36. T. A. Roth and P. Suppayak: *Mater. Sci. and Engg.*, 1978, vol. 35, p. 187.
37. L. E. Murr: *Interfacial Phenomena in Metals and Alloys*, Addison-Wesley, Reading, MA, 1975.
38. E. B. Hawbolt and L. C. Brown: *TMS-AIME*, 1967, vol. 239, p. 1916.
39. F. S. Ham: *Quart. of Appl. Math.*, 1959, vol. 17, p. 137.
40. G. Horvay and J. W. Cahn: *Acta Metall.*, 1961, vol. 9, p. 695.
41. G. Horvay and J. W. Cahn: Technical Report 60-RL-2561M, General Electric Research Laboratory, 1960.
42. E. S. K. Menon, R. W. Hyland, Jr., and H. I. Aaronson: *Scr. Metall.*, 1984, vol. 18, p. 367.
43. H. B. Aaron and H. I. Aaronson: *Acta Metall.*, 1968, vol. 16, p. 789.
44. N. A. Gjostein: *Diffusion*, H. I. Aaronson, ed., ASM, Metals Park, OH, 1973, p. 241.
45. A. M. Brown and M. F. Ashby: *Acta Metall.*, 1980, vol. 28, p. 1085.
46. A. D. Brailsford and H. B. Aaron: *J. of App. Phys.*, 1969, vol. 40, p. 1702.
47. H. I. Aaronson, C. Laird, and K. R. Kinsman: *Phase Transformations*, H. I. Aaronson, ed., ASM, Metals Park, OH, 1970, p. 313.